Atomic and Electronic Structure of Solid-Density Liquid Carbon

E. Principi,[1,*] S. Krylow,[2] M. E. Garcia,[2] A. Simoncig,[1] L. Foglia,[1] R. Mincigrucci,[1] G. Kurdi,[1] A. Gessini,[1] F. Bencivenga,[1] A. Giglia,[3] S. Nannarone,[3] and C. Masciovecchio[1]
[1]*Elettra-Sincrotrone Trieste S.C.p.A., S.S. 14 km 163.5, 34149 Basovizza (TS), Italy*
[2]*Theoretical Physics and Center for Interdisciplinary Nanostructure Science and Technology (CINSAT) Universität Kassel, Heinrich-Plett-Str. 40, 34132 Kassel, Germany*
[3]*IOM-CNR, S.S. 14, Km. 163.5, 34012 Trieste, Italy*

(Received 3 April 2020; accepted 1 September 2020; published 6 October 2020)

A liquid carbon (l-C) sample is generated through constant volume heating exposing an amorphous carbon foil to an intense ultrashort laser pulse. Time-resolved x-ray absorption spectroscopy at the C K edge is used to monitor the dynamics of the melting process revealing a subpicosecond rearrangement of the electronic structure associated with a sudden change of the C bonding hybridization. The obtained l-C sample, resulting from a nonthermal melting mechanism, reaches a transient equilibrium condition with a temperature of about 14 200 K and pressure in the order of 0.5 Mbar in about 0.3 ps, prior to hydrodynamic expansion. A detailed analysis of the atomic and electronic structure in solid-density l-C based on time-resolved x-ray absorption spectroscopy and theoretical simulations is presented. The method can be fruitfully used for extending the experimental investigation of the C phase diagram in a vast unexplored region covering the 10^3–10^4 K temperature range with pressures up to 1 Mbar.

DOI: 10.1103/PhysRevLett.125.155703

Understanding the properties of elements at high pressures and temperatures [1–4] is one of the main problems in the physics of materials under extreme conditions. The motivations to tackle such a challenging research are both technological and scientific, as for the case of carbon. Carbon and its compounds are being increasingly employed as structural materials for high temperature devices with applications in nuclear technology, space launch programs as well as for scientific instrumentation [5]. On the other hand carbon, one of the most abundant elements in the universe, can be naturally found under extreme conditions in the astrophysical context, as in planet cores [6,7]. Remarkably, research on extrasolar planets, recently rewarded with the Nobel prize in physics, has predicted [8] and demonstrated [9] the existence of carbon-based exoplanets using models developed for carbon in extreme environments.

Among the diverse condensed forms of carbon that are stable under high pressure and temperature, the liquid phase is probably the most difficult one to study. So far, many theoretical works have simulated liquid carbon (l-C), not rarely with controversial results. Calculations are aimed at shedding light on the structural properties of l-C at the atomic scale [10–16] as well as clarifying speculations about its polyamorphism [17,18]. Many efforts have been devoted to predict the phase boundaries in extended regions of the carbon phase diagram [19–22] with particular interest on the diamond-liquid coexistence line. Unfortunately, experimental corroboration of theoretical findings is still not exhaustive. Indeed, access to l-C in the laboratory under stationary conditions is practically unfeasible due to the very high melting point (about 4800 K) [19–21] and the carbon tendency to sublimate at low pressures and high temperatures [23]. These difficulties can be partially circumvented using dynamic techniques like shock-wave compression [24,25], proton- [23] and laser-driven heating [26,27]. However, typical drawbacks with these approaches are the poor time resolution, inappropriate for monitoring transient phases, as well as the scarce control of the temperature [5] and thermodynamic state of the sample. For example, surface expansion velocity in fs-laser heated a-C has been recently found in reflectivity experiments to exceed 15000 m/s [28], an order of magnitude larger than previously estimated by optical interferometry measurements [26]. Therefore, access to the sub-ps temporal window is definitely required in fs-laser heating approach to monitor the formation of l-C under controlled constant volume conditions.

In this Letter, we present a study on pressurized l-C based on time-resolved x-ray absorption spectroscopy (TRXAS) [29] measurements complemented by DFT (density functional theory)-based, two-temperature model, molecular dynamics (MD) simulations. Our approach is to reach the l-C regime through fs-laser heating [26] monitoring the formation of the liquid phase prior to hydrodynamic expansion ($t \lesssim 0.5$ ps) with a novel free electron laser (FEL) jitter-free pump-probe scheme [30]. The method gives valuable access to the sub-ps time resolution in XAS demanded for revealing ultrafast changes in the electronic structure of materials. We show

how the TRXAS technique, operated at the C K edge (284.2 eV), can be used to unveil the unknown evolution of both the near-continuum unoccupied p electronic states and sample temperature [31] upon a-C melting. The simulations, performed with the code for highly excited valence electron systems (CHIVES) [32–34], are used to predict modifications of the atomic and electronic structure of the excited C sample thus validating and complementing the information provided by TRXAS. We show, for the first time, that a solid-density l-C phase forms in the excited sample volume, about 0.3 ps after laser exposure, resulting from a nonthermal melting process and subsequent exceptionally fast thermalization of the electron and ionic subsystems. This gives us the opportunity of studying l-C under controlled conditions of temperature, pressure, and density.

The experimental part of this study has been conducted at the EIS-TIMEX beam line of the FERMI FEL facility (Trieste, Italy), complemented by additional XAS room temperature measurements of a-C [35] at the CNR-IOM BEAR beam line of the Elettra synchrotron (Trieste, Italy) [36]. In both cases, XAS has been carried out in transmission geometry. FEL TRXAS experiments were performed in single-shot pump-probe mode [26] delivering an intense laser pulse (wavelength 390 nm, duration 50–80 fs, fluence 0.4 J/cm^2) onto a self-standing amorphous carbon (a-C) foil of thickness 80 nm produced through evaporation (estimated density: 2.0 g/cm^3 [26,37,38]) by the Lebow Company. In Fig. 1(a) the XAS of room temperature a-C across the C K edge is shown as measured at the synchrotron (blue curve) and FEL (black circles). FEL XAS measurements at FERMI do not require any monochromator as the typical relative spectral bandwidth at the C K edge ($\Delta\lambda/\lambda \approx 10^{-3}$) and the fine wavelength tunability [39] are already appropriate for XAS.

Figure 1(b) shows the measured laser-induced transmission variation ($\Delta T/T$) at the FEL photon energies depicted in Fig. 1(a). In the explored spectral window (280.7–305.6 eV), including the C K edge, the transmission variation is extremely pronounced (more than 20% for some photon energies). Notably, all transmission variations of Fig. 1(b) appear to rapidly reach their asymptotic limits after about 0.5 ps. The experimental points in Fig. 1(b) are interpolated by exponential curves that are used to calculate the XAS spectrum $\alpha^*(E,t)$ for given time delays using the XAS room temperature spectrum $\alpha(E,t_0)$ as initial boundary condition. In this procedure, we assume negligible sample reflectivity (a-C refractive index is 1 for 300 eV photons [40]) thus obtaining: $\alpha = -\log(T)$. Moreover, we take into account that only a fraction of the sample foil can be efficiently heated by an intense fs-laser pump [41]. For low fluences the attenuation length of 390 nm photons in a-C is about 35 nm [42], shorter than the nominal thickness of the sample. In the applied fluence

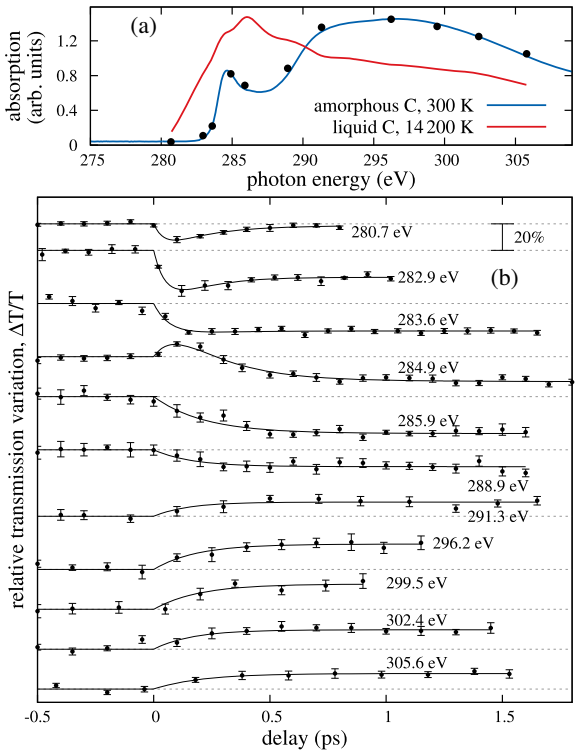

FIG. 1. (a) Solid blue line: unperturbed a-C absorption spectrum (BEAR); black circles: same spectrum measured at FERMI (EIS-TIMEX); solid red line: l-C spectrum 0.52 ps after laser exposure. (b) Time-resolved relative transmission variation, averaged over 5–15 single shot measurements, at selected FEL photon energies. Error bars are the standard deviation of the mean. Solid lines are best fit exponential curves for positive delays.

regime, the attenuation length is expected to further contract during the absorption of the pump pulse as an effect of the electron-hole plasma-induced opacity in the visible range [27]. Furthermore, XAS in transmission geometry probes both the hot front and cold rear side of the sample. Therefore we assume that, at any time, the measured spectrum $\alpha(E,t)$ is actually a linear combination of the unperturbed room temperature spectrum $\alpha(E,t_0)$ and a time-dependent hot spectrum $\alpha^*(E,t)$ [41]:

$$\alpha(E,t) = c\alpha(E,t_0) + c^*\alpha^*(E,t), \tag{1}$$

where $c = 1 - c^*$. Equation (1) is a crude approximation of the real case, tolerable as $\alpha(E,t)$ is a mean spectrum, that allows us to minimize the number of unknown parameters. The adoption of more sophisticated time-resolved temperature profiles implies more assumptions and, finally, in our opinion, does not guarantee a more realistic evaluation of the excited spectrum. Our assessment, carried out comparing the l-C unoccupied density of p states computed by CHIVES with α^* spectra for different values of c^* [43], is that the a-C specimen undergoes effective volumetric heating up to about 70% of the nominal attenuation

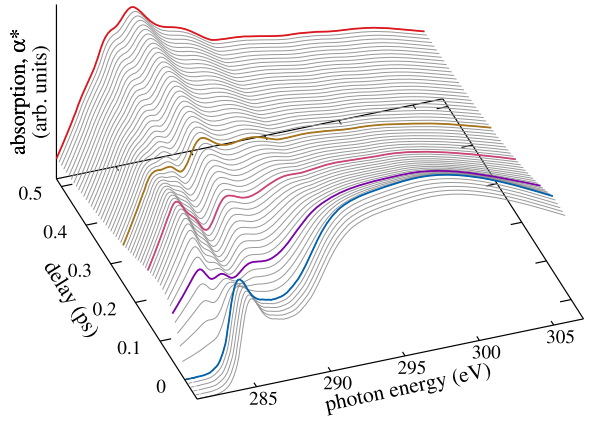

FIG. 2. Time evolution of the a-C absorption spectrum $\alpha^*(E,t)$ after laser exposure leading to l-C. Colored spectra refer to 0.0, 0.05, 0.15, 0.25, 0.52 ps time delays. Uncertainty affecting $\alpha^*(E,t)$ is around 5%.

length ($c^* = 0.31$, melting depth about 25 nm). Under these assumptions, about 50% of the pump optical energy is deposited in the excited volume leading to an average absorbed energy density of about 5 eV/atom (~40 MJ/ kg).

Figure 1(a) depicts the hot sample XAS spectrum (red curve) $\alpha^*(E,\bar{t})$, after $\bar{t} = 0.52$ ps from laser exposure, as obtained using Eq. (1). The hot spectrum profile is compatible with that of pressurized liquid carbon [26]. The temperature of the obtained l-C specimen can be fairly well estimated from the 0.21 eV^{-1} edge slope in the XAS spectrum, resulting in a temperature of about 1.2 eV (1 eV $\simeq$ 11605 K) [31,43]. Figure 2 represents in detail the time evolution of the XAS spectrum following laser excitation, reflecting the ultrafast spectral change shown in Fig. 1. The high energy part of the spectrum (> 290 eV), sensitive to sp^2 in-plane bonding abundant in a-C [16,26], gradually and monotonically decreases in less than 0.15 ps. The spectral dynamics across the K edge is affected by both the increase of sp^1 hybridization expected to be predominant in l-C [10,14] and fluctuation of the electron temperature [31]. TRXAS can not discriminate between the two processes, however the near-edge spectrum indicates that both of them take place in less than 0.5 ps. In particular, the slope of the absorption edge does not exhibit tangible changes after 0.3 ps, suggesting that the electron temperature reaches its asymptotic value in that temporal scale. From this qualitative analysis of the XAS dynamics, we deduce that the melting process of a-C occurs within a few hundreds of femtoseconds.

The nature of the revealed ultrafast spectral changes associated with the formation of a l-C sample is further investigated through the CHIVES code [34]. The computational method [43] constitutes an extension of the two-temperature-MD approach [44] to finite-temperature DFT-based MD, thus including ultrafast thermal and nonthermal effects. It is based on the local density approximation [45], atom-centered Gaussian basis set [46], relativistic pseudopotentials [47,48] and periodic boundary conditions. This approach presupposes that the electron thermalization process is widely faster than electron-phonon and phonon-phonon interactions that trigger the dynamics subject of this study. Therefore, in the simulation the electron subsystem is considered as already thermalized and the computing resources are focused on calculating the energy exchange between electrons and lattice as well as phonon-phonon interactions. The MD supercell consists of 512 carbon atoms with a density of 2.0 g/cm^3, generated using the scheme described in [49]. Excitation by a Gaussian laser pulse (FWHM: 25 fs) that leads to a final absorbed energy density of about 5.2 eV/atom was simulated by a time-dependent increase of the electron temperature. The supercell volume is kept constant during simulations to reproduce the isochoric heating experimental conditions. The response of the supercell is simulated through MD obtaining the interatomic forces as the gradients of the computed multidimensional laser excited potential energy surface (PES). The thermalization process of the electron and lattice subsystems is critically affected by the electron-phonon coupling parameter G [50] implemented in the code. The actual value of G for C under the simulated conditions is not known, therefore we have empirically set G to the value of about 17×10^{18} $Wm^{-3}K^{-1}$ that accounts for the equilibration time of about 0.3 ps deduced from TRXAS.

Figure 3(a) shows the computed dynamics of the electron and ion temperatures in the carbon sample. A nonequilibrium regime persists for about 0.3 ps, with

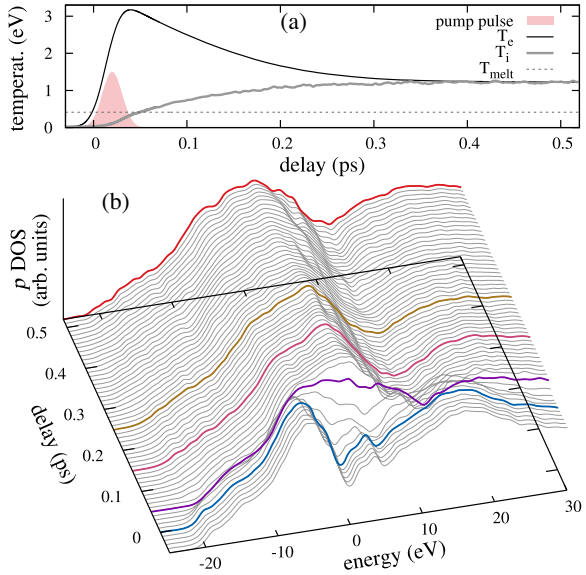

FIG. 3. CHIVES numerical simulation of fs-laser heated a-C: (a) electron (T_e) and ion temperature (T_i), nominal melting temperature of pressurized C (T_{melt}), representation of the pump pulse used in the simulations; (b) time dynamics of the pDOS across the Fermi level (set to zero in the energy scale). Colored spectra as in Fig. 2.

a maximum electron temperature of about 3.2 eV and a final equilibrium temperature of about 1.2 eV. The electron temperature rise time of about 50 fs is comparable with that of fs-laser heated Cu [51] and Ge [41]. On the contrary, the thermalization time is exceedingly faster than in Cu ($\tau > 8$ ps) and Ge ($\tau \sim 2$ ps). The calculated density of p electronic states (p DOS) shown in Fig. 3(b) undergoes a drastic rearrangement in less than 0.1 ps, consisting in a rise of the density of states across the Fermi level and a decrease 10–15 eV above that level, in very good agreement with the TRXAS findings, provided the Fermi level is set on the K edge. Notably, from Fig. 3, it is evident that the change in the electronic structure is faster than the thermalization time of the electron and ion temperatures. Actually, the onset of p-DOS changes occurs before the ion temperature reaches the nominal melting point [4800 K, 0.414 eV, dashed line in Fig. 3(a)].

We obtain the unoccupied p-DOS states of C for a given time delay by multiplying the p DOS computed with CHIVES [Figs. 3(b) and 4(b)] by $1 - f(E)$, where $f(E)$ is the Fermi-Dirac electron distribution function [Fig. 4(a)] [29]. For this calculation, DFT-based simulations with CHIVES indicate that the chemical potential in $f(E)$ can be considered as a constant. Figure 4(c) shows the unoccupied p DOS of l-C for $t = 0.52$ ps, convoluted with a Gaussian of 0.3 eV FWHM to account for the experimental resolution broadening which is expected to be larger than the s core hole lifetime broadening in carbon. K-edge XAS directly probes, for dipole selection rules, the unoccupied p DOS that approaches, in C, the total DOS across the Fermi level. Core-hole exciton effects are likely suppressed by Coulomb screening, especially after sample ultrafast melting and concomitant massive electron delocalization, therefore the absorption spectra mainly reflect the profile of the unoccupied p DOS. Calculation of time-dependent transition dipole matrix elements is not included in the simulations as computationally unachievable. In Fig. 4(c) the l-C absorption spectrum (subjected to removal of linear preedge absorption background, energy offset of 283.2 eV and finally scaled by a factor 0.011) nicely matches the calculated unoccupied p DOS across the Fermi level, indicating that both the electronic structure and temperature value computed by CHIVES for l-C are realistic. Effective pressure exerted on a sample upon isochoric laser heating is mainly due to the anharmonic ionic motion [27]. A carbon sample with density 2.0 g/cm^3 subjected to constant volume heating up to a temperature of 1.2 eV, is expected to reach a pressure of about 0.5 Mbar [27,43]. Those thermodynamic conditions persist in the bulk part of the excited sample volume for some hundreds of femtoseconds [27,28] that is the time window explored in this study.

The transformation of the electronic structure revealed by TRXAS and CHIVES induces a profound ultrafast rearrangement of the local atomic structure. Figure 5 presents a summary of the evolution of relevant physical quantities associated with the carbon atomic structure, computed by CHIVES. Figures 5(a) and 5(c) show the pair $g_2(r)$ and angular $g_3(\theta)$ distribution function,

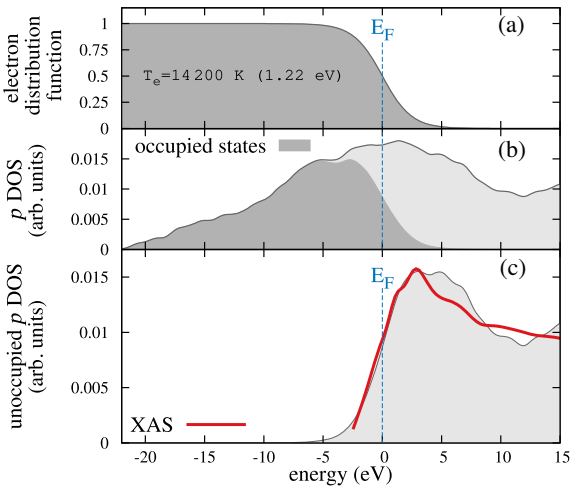

FIG. 4. CHIVES calculations on l-C 0.52 ps after laser pump exposure: (a) electron distribution function (Fermi-Dirac) from Fig. 3(a); (b) related p DOS and occupied electronic states; (c) unoccupied p DOS compared with scaled TRXAS of l-C, $\alpha^*(E, \bar{t})$, $\bar{t} = 0.52$ ps [Fig. 1(a)].

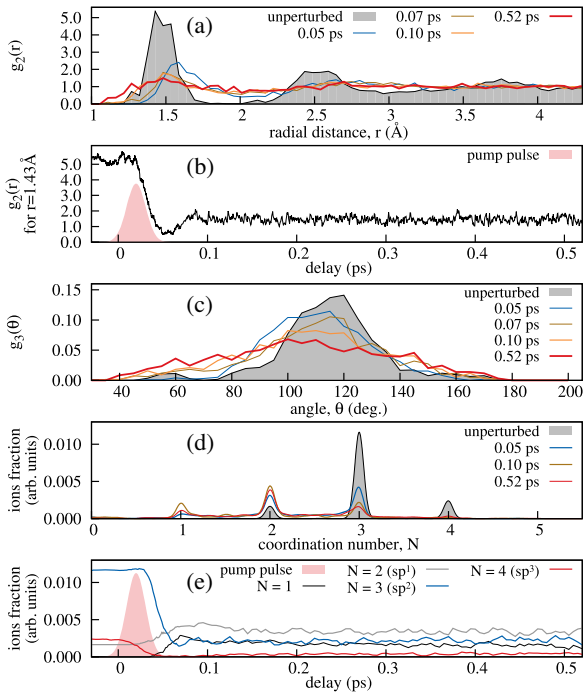

FIG. 5. CHIVES calculations: (a) pair correlation function $g_2(r)$; (b) height of the first peak; $g_2(r_0)$, $r_0 = 1.43$ Å; (c) angular distribution function $g_3(\theta)$; (d) ion distribution as a function of the coordination number; (e) height of the main peaks in panel "d."

respectively. Disordering of the atomic structure is already evident after 0.05 ps associated with both a pronounced broadening of the g_2 and g_3 main peaks and the stretching of the first neighbor average distance from 1.47 to 1.62 nm. After only 0.07 ps, the g_2 profile resembles that of a liquid. Further adjustment of g_2 (compression of the first neighbor distance to about 1.5 Å) and g_3 distributions (additional broadening) is noticeable between 0.1 and 0.5 ps upon thermalization of the electron and lattice subsystem and related pressurization. Figure 5(b) shows the time evolution of the first peak height of g_2 indicating that the local atomic order rearranges simultaneously with the electronic structure as reported in Fig. 3(b). Figures 5(d) and 5(e) show how the coordination number evolves in time, providing confirmation of the TRXAS qualitative analysis. The sp^2 hybridization of the a-C structure rapidly disappears triggering the ultrafast structural rearrangement reported in Figs. 5(a) and 5(c) that leads to l-C with a prevalence of sp^1 hybridization. Experimental and theoretical findings indicate that the time scale for a-C melting is about 0.1 ps, well before completion of the energy transfer from electrons to ions. Moreover, calculations indicate that melting initiates prior to a significant lattice temperature increase. Consequently, the nature of the observed melting dynamics is likely nonthermal. This means that the local atomic order in a-C, dominated by sp^2 bonding, collapses as a consequence of the ultrafast PES modification and rapid increase of free electron density, similarly to what occurs in semiconductors [52,53].

In conclusion, employing our combined experimental and theoretical approach, we succeeded in obtaining access to the electronic and atomic structure of liquid carbon at about 1.2 eV (14 200 K), 0.5 Mbar and 2.0 g/cm^3. Under those extreme conditions, monitored by FEL XAS with unprecedented sub-ps time resolution, the atomic structure of l-C is dominated by chainlike structures, resulting from sp^1 hybridization, with average C-C distance of about 1.5 Å. The electron distribution is well described, also under nonequilibrium regime, by a Fermi-Dirac function with constant chemical potential. The abundance of unsaturated bonds and related high density of states across the Fermi level indicate that the liquid has metallic character. Our study reveals that fs-laser-driven l-C results from ultrafast nonthermal melting of a-C, occurring in about 0.1 ps, probably without superheating of the ion subsystem. The collapse of the local atomic order is a direct and immediate consequence of the rearrangement of the electronic structure and the related PES. Notably, the electronic and atomic temperatures equilibrate in about 0.3 ps, exceptionally faster than in other laser heated materials, thus leading to the formation of l-C under constant volume conditions. This offers the unique opportunity to create and monitor l-C under a well-defined thermodynamic state, prior to activation of the hydrodynamic expansion and pressure release in the excited sample volume [26–28]. The observed thermalization dynamics can be simulated using a constant electron-phonon coupling parameter of about 17×10^{18} Wm^{-3} K^{-1}, significantly larger than for other excited metals [50]. We finally emphasize that sub-ps TRXAS, combined with isochoric heating of different C allotropes, can give access to the electronic structure of l-C in a vast region of the phase diagram with pressures in the range 0.1–1 Mbar and temperatures greater than several eV.

The FERMI team (FEL, seed laser, beam transport) is acknowledged for its invaluable assistance during the experiment. E. P. thanks Professor S. L. Johnson (PSI, ETH Zurich) for his fruitful comments on preliminary experimental results. M. E. G. acknowledges financial support by the Deutsche Forschungsgemeinschaft through Grant No. GA 465/18-1. The MD simulations were performed at the Lichtenberg Super Computer Facility of the TU-Darmstadt (Germany).

*emiliano.principi@elettra.eu

[1] S. Anzellini, V. Monteseguro, E. Bandiello, A. Dewaele, L. Burakovsky, and D. Errandonea, Sci. Rep. **9**, 13034 (2019).
[2] G. Weck, V. Recoules, J.-A. Queyroux, F. Datchi, J. Bouchet, S. Ninet, G. Garbarino, M. Mezouar, and P. Loubeyre, Phys. Rev. B **101**, 014106 (2020).
[3] D. Errandonea, S. G. MacLeod, L. Burakovsky, D. Santamaria-Perez, J. E. Proctor, H. Cynn, and M. Mezouar, Phys. Rev. B **100**, 094111 (2019).
[4] R. Briggs, F. Coppari, M. G. Gorman, R. F. Smith, S. J. Tracy, A. L. Coleman, A. Fernandez-Pañella, M. Millot, J. H. Eggert, and D. E. Fratanduono, Phys. Rev. Lett. **123**, 045701 (2019).
[5] A. Savvatimskiy, *Carbon at High Temperatures* (Springer, New York, 2015).
[6] L. R. Benedetti, J. H. Nguyen, W. A. Caldwell, H. Liu, M. Kruger, and R. Jeanloz, Science **286**, 100 (1999).
[7] M. Ross, Nature (London) **292**, 435 (1981).
[8] M. J. Kuchner and S. Seager, arXiv:astro-ph/0504214.
[9] N. Madhusudhan, J. Harrington, K. Stevenson, S. Nymeyer, C. Campo, P. Wheatley, D. Deming, J. Blecic, R. Hardy, N. Lust, D. Anderson, A. Collier-Cameron, C. Britt, W. Bowman, L. Hebb, C. Hellier, P. Maxted, D. Pollacco, and R. West, Nature (London) **469**, 64 (2011).
[10] V. Dozhdikov, A. Basharin, P. Levashov, and D. Minakov, J. Chem. Phys. **147**, 214302 (2017).
[11] L. X. Benedict, K. P. Driver, S. Hamel, B. Militzer, T. Qi, A. A. Correa, A. Saul, and E. Schwegler, Phys. Rev. B **89**, 224109 (2014).
[12] M. E. Garcia and H. O. Jeschke, Appl. Surf. Sci. **208–209**, 61 (2003).
[13] H. O. Jeschke, M. E. Garcia, and K. H. Bennemann, Phys. Rev. Lett. **87**, 015003 (2001).
[14] J. N. Glosli and F. H. Ree, Phys. Rev. Lett. **82**, 4659 (1999).
[15] C. Z. Wang, K. M. Ho, and C. T. Chan, Phys. Rev. B **47**, 14835 (1993).
[16] G. Galli, R. M. Martin, R. Car, and M. Parrinello, Phys. Rev. Lett. **62**, 555 (1989).

[17] Y. He, H. Li, Y. Jiang, X. Li, and X. Bian, Sci. Rep. **4**, 3635 (2014).

[18] C. J. Wu, J. N. Glosli, G. Galli, and F. H. Ree, Phys. Rev. Lett. **89**, 135701 (2002).

[19] A. Correa, S. Bonev, and G. Galli, Proc. Natl. Acad. Sci. U.S.A. **103**, 1204 (2006).

[20] X. Wang, S. Scandolo, and R. Car, Phys. Rev. Lett. **95**, 185701 (2005).

[21] L. M. Ghiringhelli, J. H. Los, E. J. Meijer, A. Fasolino, and D. Frenkel, Phys. Rev. Lett. **94**, 145701 (2005).

[22] M. P. Grumbach and R. M. Martin, Phys. Rev. B **54**, 15730 (1996).

[23] A. Pelka, G. Gregori, D. O. Gericke, J. Vorberger, S. H. Glenzer, M. M. Günther, K. Harres, R. Heathcote, A. L. Kritcher, N. L. Kugland, B. Li, M. Makita, J. Mithen, D. Neely, C. Niemann, A. Otten, D. Riley, G. Schaumann, M. Schollmeier, An. Tauschwitz, and M. Roth, Phys. Rev. Lett. **105**, 265701 (2010).

[24] D. Kraus, J. Vorberger, D. O. Gericke, V. Bagnoud, A. Blažević, W. Cayzac, A. Frank, G. Gregori, A. Ortner, A. Otten, F. Roth, G. Schaumann, D. Schumacher, K. Siegenthaler, F. Wagner, K. Wünsch, and M. Roth, Phys. Rev. Lett. **111**, 255501 (2013).

[25] M. Knudson, M. Desjarlais, and D. Dolan, Science **322**, 1822 (2008).

[26] S. L. Johnson, P. A. Heimann, A. G. MacPhee, A. M. Lindenberg, O. R. Monteiro, Z. Chang, R. W. Lee, and R. W. Falcone, Phys. Rev. Lett. **94**, 057407 (2005).

[27] D. H. Reitze, H. Ahn, and M. C. Downer, Phys. Rev. B **45**, 2677 (1992).

[28] R. Mincigrucci, E. Principi, F. Bencivenga, L. Foglia, A. Gessini, G. Kurdi, A. Simoncig, and C. Masciovecchio, Photonics **4**, 23 (2017).

[29] F. Dorchies and V. Recoules, Phys. Rep. **657**, 1 (2016).

[30] M. B. Danailov, F. Bencivenga, F. Capotondi, F. Casolari, P. Cinquegrana, A. Demidovich, E. Giangrisostomi, M. P. Kiskinova, G. Kurdi, M. Manfredda, C. Masciovecchio, R. Mincigrucci, I. P. Nikolov, E. Pedersoli, E. Principi, and P. Sigalotti, Opt. Express **22**, 12869 (2014).

[31] F. Dorchies, F. Festa, V. Recoules, O. Peyrusse, A. Benuzzi-Mounaix, E. Brambrink, A. Levy, A. Ravasio, M. Koenig, T. Hall, and S. Mazevet, Phys. Rev. B **92**, 085117 (2015).

[32] E. S. Zijlstra, A. Kalitsov, T. Zier, and M. E. Garcia, Phys. Rev. X **3**, 011005 (2013).

[33] E. S. Zijlstra, A. Kalitsov, T. Zier, and M. E. Garcia, Adv. Mater. **25**, 5605 (2013).

[34] E. S. Zijlstra, T. Zier, B. Bauerhenne, S. Krylow, P. M. Geiger, and M. E. Garcia, Appl. Phys. A **114**, 1 (2014).

[35] J. Díaz, S. Anders, X. Zhou, E. J. Moler, S. A. Kellar, and Z. Hussain, Phys. Rev. B **64**, 125204 (2001).

[36] CNR-IOM BEAR beam line (2020) http://www.elettra.trieste.it/elettra-beamlines/bear.html.

[37] J. Robertson, Prog. Solid State Chem. **21**, 199 (1991).

[38] G. Galli, R. M. Martin, R. Car, and M. Parrinello, Phys. Rev. B **42**, 7470 (1990).

[39] E. Allaria *et al.*, New J. Phys. **14**, 113009 (2012).

[40] H.-J. Hagemann, W. Gudat, and C. Kunz, J. Opt. Soc. Am. **65**, 742 (1975).

[41] E. Principi, E. Giangrisostomi, R. Mincigrucci, M. Beye, G. Kurdi, R. Cucini, A. Gessini, F. Bencivenga, and C. Masciovecchio, Phys. Rev. B **97**, 174107 (2018).

[42] E. T. Arakawa, M. W. Williams, and T. Inagaki, J. Appl. Phys. **48**, 3176 (1977).

[43] See the Supplemental Material at http://link.aps.org/supplemental/10.1103/PhysRevLett.125.155703 for details on raw data reduction, temperature and pressure evaluation, numerical calculations and other aspects of the data analysis

[44] D. S. Ivanov and L. V. Zhigilei, Phys. Rev. B **68**, 064114 (2003).

[45] J. P. Perdew and Y. Wang, Phys. Rev. B **45**, 13244 (1992).

[46] E. S. Zijlstra, N. Huntemann, A. Kalitsov, M. E. Garcia, and U. von Barth, Model. Simul. Mater. Sci. Eng. **17**, 015009 (2008).

[47] S. Goedecker, M. Teter, and J. Hutter, Phys. Rev. B **54**, 1703 (1996).

[48] C. Hartwigsen, S. Goedecker, and J. Hutter, Phys. Rev. B **58**, 3641 (1998).

[49] J. Han, W. Gao, J. Zhu, S. Meng, and W. Zheng, Phys. Rev. B **75**, 155418 (2007).

[50] Z. Lin, L. V. Zhigilei, and V. Celli, Phys. Rev. B **77**, 075133 (2008).

[51] B. Mahieu, N. Jourdain, K. Ta Phuoc, F. Dorchies, J.-P. Goddet, A. Lifschitz, P. Renaudin, and L. Lecherbourg, Nat. Commun. **9**, 3276 (2018).

[52] K. Sokolowski-Tinten, J. Solis, J. Bialkowski, J. Siegel, C. N. Afonso, and D. von der Linde, Phys. Rev. Lett. **81**, 3679 (1998).

[53] A. Rousse, C. Rischel, S. Fourmaux, I. Uschmann, S. Sebban, G. Grillon, P. Balcou, E. Frster, J. Geindre, P. Audebert, J. Gauthier, and D. Hulin, Nature (London) **410**, 65 (2001).